

## Analysis of the potential of ICRF waves to heat bulk ions in DEMO

D. Gallart<sup>1</sup>, M.J. Mantsinen<sup>1,2</sup>, Y. Kazakov<sup>3</sup>

<sup>1</sup> *Barcelona Supercomputing Center, Barcelona, Spain*

<sup>2</sup> *Catalan Institution for Research and Advanced Studies, Barcelona, Spain*

<sup>3</sup> *Laboratory for Plasma Physics, LPP-ERM/KMS, Brussels, Belgium*

**Introduction** Among the auxiliary heating schemes presently envisaged for ITER, heating with waves in the ion cyclotron range of frequencies (ICRF) is the only scheme that can provide dominant bulk ion heating. Ion heating with ICRF waves results from the absorption of the wave power  $P_{ICRF}$  by resonant ions  $P_i$  which can subsequently transfer their energy to the fuel ions via collisions (Fig. 1). This effect is in competition with direct electron damping  $P_e$  and other mechanisms which can also damp the wave power. Bulk ion heating dominates provided

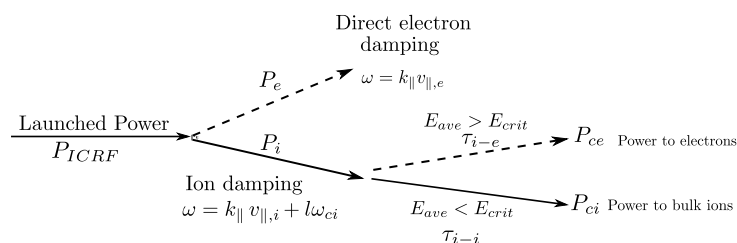


Figure 1: *Scheme of the power deposition in the ICRF heating process.*

that the energy of the resonant ions  $E_{ave}$  is tailored to remain below the critical energy  $E_{crit}$  at which they transfer energy equally to electrons  $P_{ce}$  and ions  $P_{ci}$  in collisions. Fast ions transfer their energy via collisions to bulk ions and electrons on the time scale of the slowing-down times on ions  $\tau_{i-i}$  and electrons  $\tau_{i-e}$ . For fast  $^3\text{He}$  ions and tritons, which will be the main ICRF-resonant ion species in ITER,  $\tau_{i-i}$  is 1 ms and 3 ms and  $\tau_{i-e} = 1$  s and 3.4 s, respectively, at typical steady-state ITER parameters. The bulk ion heating capabilities of ICRF waves in ITER have been studied e.g. in Refs. [1, 2]. We analyze the potential of ICRF waves to heat the fuel D-T ions in DEMO. DEMO is a proposed nuclear fusion demonstration power plant that is expected to be built after ITER. While ITER's main purpose is to confirm the feasibility of nuclear fusion as an energy source, DEMO is planned as the first fusion reactor to produce net electrical energy. Our analysis is carried out for the DEMO 2015 (from now on DEMO2), using the ICRF modelling codes PION [3] and TORIC [4]. We also have analyzed the previous design DEMO 2013 (from now on DEMO1) see Ref. [5].

**Analysis of bulk ion heating in DEMO** We concentrate our studies on the second harmonic ICRF heating of tritium with and without  $^3\text{He}$  in a 50%:50% D-T plasma in DEMO. The ICRF scenario is for a standard low-field side (LFS) midplane launch with thermal plasma (there is

Design	$R_0(m)$	$a(m)$	$B(T)$	$I_p(MA)$	$\kappa$	$\delta$	Plas. Vol. ( $m^3$ )	Fusion P. (MW)
DEMO1	9.25	2.64	6.8	18.6	1.52	0.33	2009	2119
DEMO2	9.07	2.93	5.7	19.6	1.59	0.33	2502	2037

Table 1: DEMO1 and DEMO2 parameters.

no ICRF+NBI interaction) and a fixed toroidal mode number ( $N_\phi \simeq Rk_\parallel$ ).  $P_{ICRF} = 100$  MW is considered as a baseline value of the coupled ICRF power. The basic parameters of the ICRF system are summarized in Table 2 for both DEMO designs. The study has consisted of a scan of the electron density  $n_e$  and the electron temperature  $T_e$ . In order to compare both DEMO designs from the bulk ion heating point of view, several simulations have been made for both designs at the same DEMO design point (DEMO1). Simulations show that direct electron damping grows as  $n_e$  and  $T_e$  increase but also and more strongly as the magnetic field  $B$  decreases, see Ref. [6]. For the same  $N_\phi$  DEMO1 showed higher bulk ion heating than DEMO2.

Parameter	DEMO1	DEMO2
Toroidal magnetic field $B$ (T)	6.8	5.7
ICRF frequency (MHz)	66, 70, 74	54, 57, 61
Resonance location ( $\frac{r_{res}}{a}$ )	0.2, -0.05, -0.2	0.2, -0.05, -0.2
ICRF Power (MW)	100	100
Toroidal mode number $N_\phi$	50	50
DEMO design point $n_e$ ( $m^{-3}$ ), $T_e$ (keV)	$1.2 \cdot 10^{20}$ , 30	$1.0 \cdot 10^{20}$ , 27.4

Table 2: ICRF parameters for DEMO.

**<sup>3</sup>He minority heating** In this case, the frequency of the wave has been set equal to the fundamental harmonic of <sup>3</sup>He,  $\omega = \omega_{^3He} = 2\omega_T$ , for central resonance  $f = 57.6$  MHz. The

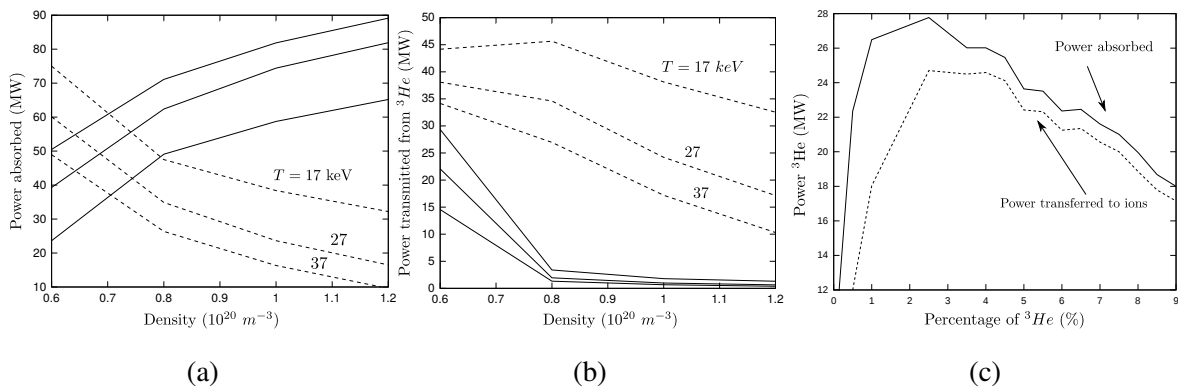


Figure 2: For central resonance  $f = 57.6$  MHz. (a) Scan in  $T_e$  and  $n_e$  of the power absorbed by <sup>3</sup>He (dashed line) and electrons (solid line). (b) Power transferred by <sup>3</sup>He to bulk ions (dashed) and to electrons (solid). (c) Power absorption by <sup>3</sup>He and power transferred to ions by <sup>3</sup>He for different concentrations at  $n_e = 1.0 \cdot 10^{20} m^{-3}$ .

power absorbed by <sup>3</sup>He tends to decrease as temperature  $T_e$  and electron density  $n_e$  increase. In

fact, for densities  $n_e \geq 0.8 \cdot 10^{20} \text{ m}^{-3}$  direct electron damping clearly dominates (Fig. 2a). Only for low densities  $n_e \sim 0.6 \cdot 10^{20} \text{ m}^{-3}$  the energy of fast ions is considerably high and relatively close to  $E_{crit}$ . The power transferred to electrons from  $^3\text{He}$  is only important for low densities (Fig. 2b), as  $n_e$  increases the average fast ion energy is much smaller than  $E_{crit}$  and therefore, for  $n_e \geq 0.8 \cdot 10^{20} \text{ m}^{-3}$  the power transferred to electrons is negligible. At the DEMO design point the slowing-down times of fast  $^3\text{He}$  ions are  $\tau_{i-i} = 8.5 \cdot 10^{-3} \text{ s}$  and  $\tau_{i-e} = 1.1 \text{ s}$ .

The dependence of bulk ion heating on the  $^3\text{He}$  concentration for the DEMO design point shows two different regions (Fig. 2c). Firstly, for low concentrations, the power transferred is considerably lower than the power absorbed as the energy of fast ions is high. In this region as the concentration of  $^3\text{He}$  increases the polarization of the wave is enhanced and therefore, the power absorbed and transferred becomes stronger. At  $\sim 3\%$  of  $^3\text{He}$  concentration a maximum is reached. Beyond this maximum the wave polarization becomes increasingly unfavorable as the concentration increases, and consequently, the power absorbed and transferred by  $^3\text{He}$  decreases. However, the difference between the two curves is due to the average fast ion energy which is 500 keV and 131 keV for 0.5% and 5% concentrations, respectively.

**Second harmonic tritium scenario** This scenario has two main advantages in comparison with  $^3\text{He}$  minority heating. Firstly, that no  $^3\text{He}$  is required and secondly, there is no dilution by  $^3\text{He}$ . Therefore, the fusion rate D+T is higher than for  $^3\text{He}$  dilution (Fig. 3a). The power absorption (Fig. 3b) follows a similar trend as in the  $^3\text{He}$  minority scenario (Fig. 2a). The power transferred from tritium to bulk ions does not change considerably for different  $n_e$  (Fig. 3c) because average fast ions energy changes substantially from low densities to high densities. For low densities the average fast ion energy is larger than  $E_{crit}$  and the power is mainly transferred to electrons while for high densities it is lower than  $E_{crit}$ . This change in  $E_{ave}$  with respect to  $E_{crit}$ , together with the decrease in absorbed power by tritons (Fig. 3b), results in a relatively constant power transfer to bulk ions as function of  $n_e$ . The power transferred by fast tritium ions to bulk ions for low densities is lower than the power transferred by  $^3\text{He}$  (Fig. 2b), 25 MW and 40 MW respectively. This difference is important for the start up where low densities are used and good bulk ion heating is needed. As the electron density grows the average fast ion energy decreases and bulk ion heating dominates for densities  $n_e \geq 1.0 \cdot 10^{20} \text{ m}^{-3}$ . At the DEMO design point the slowing-down times of fast tritium ions are  $\tau_{i-i} = 3.6 \cdot 10^{-2} \text{ s}$  and  $\tau_{i-e} = 4.6 \text{ s}$ . The power transferred to bulk ions at the DEMO design point is 24.8 MW which is more than for minority heating scenario (22.4 MW).

**Off-axis heating** The results shown above are computed for a frequency of 57.6 MHz, which places the resonance in the center of the plasma. We have also carried out simulations with

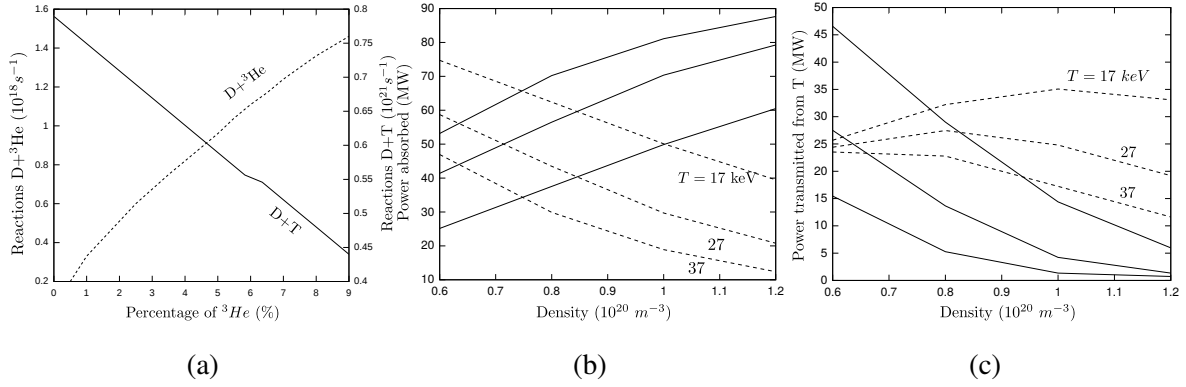


**Figure 3:** For central resonance  $f = 57.6\text{ MHz}$  (a) Fusion reaction rates for different concentrations of  ${}^3\text{He}$ . (b) Scan in  $T_e$  and  $n_e$  of the power absorbed by tritium (dashed line) and electrons (solid line). (c) Power transferred by tritium to bulk ions (dashed) and to electrons (solid).

the off-axis resonance locations,  $r/a = 0.2$  and  $-0.2$ , corresponding to a wave frequency of  $54.0\text{ MHz}$  and  $61.7\text{ MHz}$ , respectively. The results are presented in Table 3. The bulk ion heating fraction by ICRF can be maximized in DEMO by placing the ICRF resonance slightly off-axis on the low-field side to minimize the competing direct electron damping. The  $k_{\parallel}$  used in this analysis is in line with earlier works on ICRF current drive for DEMO, cf. Ref. [7]. Further steps will consist of an analysis of lower  $k_{\parallel}$ , where an increased power transfer to bulk ions is expected due to weaker direct electron damping, and studying the possibility to heat heavy impurity ions such as  ${}^9\text{Be}$  or  ${}^7\text{Li}$  via the three-ion ICRF mechanism suggested in Ref. [8].

Composition	54 MHz	58 MHz	62 MHz
${}^3\text{He}$ 5%	42.9 MW	22.4 MW	14.3 MW
T	40.8 MW	24.8 MW	8.6 MW

Table 3: Power transferred to bulk ions ( $P_{\text{ICRF}} = 100\text{ MW}$ ).

**Acknowledgments** This work has been carried out within the framework of the EUROfusion Consortium and has received funding from the Euratom research and training programme 2014-2018 under grant agreement No 633053. The views and opinions expressed herein do not necessarily reflect those of the European Commission. We are grateful to Dr. R. Wenninger and Dipl.-Ing T. Franke (PPPT, Garching) for DEMO parameters.

## References

- [1] V. Bergeaud, L.-G. Eriksson and D.F.H. Start, Nuclear Fusion **40**, 35 (2000).
- [2] R.J. Dumont and D. Zaroso, Nuclear Fusion **53**, 013002 (2013).
- [3] L.-G. Eriksson, T. Hellsten and U. Willén, Nuclear Fusion **33**, 1037 (1993).
- [4] M. Brambilla and R. Bilato, Nuclear Fusion **46**, S387 (2006).
- [5] D. Gallart, M. J. Mantsinen, Y. Kazakov, Radio Frequency Power in Plasmas, AIP conf. proceed., (2015).
- [6] A. Becoulet, Plasma Phys. Control. Fusion **38**, A1-A11 (1996).
- [7] Ye.O. Kazakov et al., Plasma Phys. Control. Fusion **57**, 025014 (2015).
- [8] Ye.O. Kazakov et al., Nucl. Fusion **55**, 032001 (2015).